Theory of thermoelectric power factor in quantum well and quantum wire superlattices

D. A. Broido
Department of Physics, Boston College, Chestnut Hill, Massachusetts 02467

T. L. Reinecke
Naval Research Laboratory, Washington, District of Columbia 20375

(Received 16 February 2001; published 2 July 2001)

Calculations are presented for thermoelectric transport in quantum well and quantum wire superlattices, using (i), the full superlattice electronic band structure in (ii) a multisubband inelastic Boltzmann equation for carrier-phonon scattering. The transport direction is taken to be in the quantum well planes and along quantum wires. It is demonstrated that these two features are needed to give a quantitative treatment of the power factor P in superlattice systems. Results are given for PbTe and for GaAs quantum well and quantum wire superlattices, including the dependence of P on growth direction and on potential offset. For both quantum well and quantum wire superlattices, the dependence of P on potential offset V_0 is found to be qualitatively weaker than in previous work based on the constant relaxation time approximation for carrier scattering. These weaker dependences on V_0 are traced mainly to the enhancement of the electron-phonon scattering rates upon confinement. These results give a different picture of the effects of confinement on P suggesting, for example, that increased confinement in superlattices does not lead to significantly higher P and that free-standing structures, such as free-standing quantum wires, may be particularly attractive for thermoelectric applications.

DOI: 10.1103/PhysRevB.64.045324 PACS number(s): 73.50.Bk, 73.50.Lw, 73.50.Dn

I. INTRODUCTION

There has been renewed interest in recent years in understanding the thermoelectric transport properties of low-dimensional semiconductor systems such as quantum well and quantum wire superlattices. This has been motivated in part by the interest in finding materials and systems for use in cleaner, more efficient cooling and power generation applications.[1] The desirability of a material for use in such systems is characterized by the dimensionless ''figure of merit''[2]

$$ZT = \frac{P}{\kappa} T. \tag{1}$$

Here, T is the temperature, $P = \sigma S^2$ is the power factor, with σ the electrical conductivity and S the Seebeck coefficient, and κ is the thermal conductivity $\kappa = \kappa_e + \kappa_L$, which consists of two components κ_e and κ_L corresponding to the carrier and lattice contributions, respectively. In the past few decades, little improvement in the figure of merit of bulk materials has been realized. Room temperature values of the dimensionless figure of merit ZT for the bulk semiconductor Bi_2Te_3 are the highest known to date, with $ZT \approx 1$.

Interest in the potential of quantum well and quantum wire superlattices for thermoelectric applications has been motivated in part by the prospect that these systems might have high power factors and figures of merit. The first calculations of the power factor and the figure of merit Z in quantum well and quantum wire systems[3,4] focused on the effect on these quantities of the change in the electronic density of states resulting from the reduced dimensionality. These calculations attracted considerable attention because of the prediction of dramatic enhancements in P and Z with decreasing well and wire dimension. The model systems[3,4] used in these calculations were taken to have infinite confining potentials (no barrier layers), and the carrier scattering was represented within a constant relaxation time approximation (CRTA). In later work, the effects of barrier layers with finite potential offsets were included using a Kronig-Penny description of the electronic band structure but still treating carrier scattering within the CRTA.[5–7] In the resulting picture, P increased from its bulk value for decreasing well and wire widths, reaching a maximum and then decreasing due to tunneling through the barriers. In that work, the maximum value of P was found to increase substantially with increasing potential barrier height.

Recent measurements on PbTe multiple quantum well structures[8,9] demonstrated that enhanced power factors could be achieved, thus stimulating further experimental and theoretical research on the thermoelectric properties of quantum well and wire systems. These measurements were for individual conducting layers, and not for the full three-dimensional (3D) structure including the barrier layers. In subsequent calculations for PbTe [111] quantum wells with infinite potential offsets,[10] we included the multivalley anisotropic PbTe band structure and a realistic treatment of carrier scattering processes beyond the CRTA. In that work, we found that P *decreased* below the bulk value for narrow wells due mainly to the strong lifting of the fourfold valley degeneracy in PbTe wells produced by confinement and also because of strongly enhanced scattering rates with decreasing well size. Subsequent calculations of P have been performed for single PbTe quantum wells[11] to address the experimental results of Refs. 8 and 9. However, the formulations in Refs. 10 and 11 cannot describe the power factor for realistic superlattices with finite potential barrier

heights, which are characterized by anisotropic and nonparabolic band structure along the superlattice directions.

In the present paper, we give a quantitative treatment of thermoelectric transport in quantum well and quantum wire superlattices. The transport direction is taken to be in the planes of quantum wells and along the quantum wires. Full superlattice band structure calculations are given for the electronic states and incorporated in a solution of the inelastic 3D Boltzmann equation. Detailed results are given for GaAs and PbTe quantum well and wire superlattice systems. These materials are chosen in part to examine the dependence of P on systems with different band structures and different dominant carrier scattering mechanisms. Qualitatively different features are obtained here which are broadly applicable to semiconductor superlattice systems. In particular, the power factor for both materials is found to depend only weakly on barrier height for quantum well and wire superlattices in contrast to results obtained in the CRTA.[5–7] This work also suggests that free-standing quantum wire structures may be promising candidate systems for thermoelectric applications.

In Sec. II, the theory for calculating the electrical conductivity and the Seebeck coefficient for in-plane thermoelectric transport in quantum well superlattices is presented. Section III presents the corresponding theory for thermoelectric transport along quantum wire superlattices. The results for the power factor in quantum well and quantum wire superlattices are given in Sec. IV.

II. THERMOELECTRIC TRANSPORT IN QUANTUM WELL SUPERLATTICES

We consider thermoelectric transport in a quantum well superlattice with well width a, barrier width b, period $d=a+b$, and potential barrier height V_0. We take the growth axis in the z direction. The state of the electron is specified by subband index n and wave vector $\mathbf{k}=(\mathbf{k}_\parallel,k_z)$, where $\mathbf{k}_\parallel=(k_x,k_y)$ is the in-plane component. The Boltzmann equation for the superlattice for steady state electron transport in the presence of electric field $\mathbf{E}$ and temperature gradient $\boldsymbol{\nabla} T$ is[12]

$$-\frac{e\mathbf{E}}{\hbar}\cdot\boldsymbol{\nabla}_k f_n+\frac{\boldsymbol{\nabla}_k\epsilon_n}{\hbar}\cdot\boldsymbol{\nabla} T\frac{\partial f_n}{\partial T}=\left.\frac{\partial f_n}{\partial t}\right|_c, \tag{2}$$

$$\left.\frac{\partial f_n}{\partial t}\right|_c=\frac{V}{8\pi^3}\sum_{n'}\int d\mathbf{k}'\{W_{n'n}(\mathbf{k}',\mathbf{k})f_{n'}(\mathbf{k}')[1-f_n(\mathbf{k})] - W_{nn'}(\mathbf{k},\mathbf{k}')f_n(\mathbf{k})[1-f_{n'}(\mathbf{k}')]\}. \tag{3}$$

Here, $f_n(\mathbf{k},\mathbf{r})$ is the distribution function for electrons in superlattice state $(n,\mathbf{k})$, $W_{nn'}(\mathbf{k},\mathbf{k}')$ is the scattering rate taking electrons from state $(n,\mathbf{k})$ to state $(n',\mathbf{k}')$, and $\epsilon_n(\mathbf{k})$ is the electron energy. The collision operator $\partial f_n/\partial t|_c$ accounts for intra-and intersubband inelastic scattering into and out of the state $(n,\mathbf{k})$.

We focus on thermoelectric transport in the plane of the quantum well layers, which is the direction of interest in most of the experimental and theoretical work to date. Materials of interest for thermoelectric applications are typically characterized by multiple ellipsoidal conduction band valleys. Within the effective-mass approximation, the quantum well superlattice subband structure deriving from each bulk valley can be described by a superlattice dispersion along the confinement direction, taken to be the z direction, and by an in-plane parabolic but anisotropic subband dispersion. Thus, for each valley,

$$\epsilon_n(\mathbf{k})=\epsilon_n(k_z)+\frac{\hbar^2}{2}\left(\frac{k_x^2}{m_x}+\frac{k_y^2}{m_y}\right). \tag{4}$$

Here, $\epsilon_n(k_z)$ is the superlattice dispersion for each valley, which is obtained, along with the superlattice Bloch functions $\psi_{nk_z}(z)$, by numerical solution of the Schrödinger equation for the Kronig-Penny potential with offset V_0.

We calculate the contribution to the thermoelectric transport coefficients from the occupied subbands deriving from each valley and sum these contributions to obtain the full results. Intervalley scattering is neglected so that each valley is treated independently. For notational simplicity, the valley index is omitted in the expressions presented below. For each valley, we choose the x and y directions to be oriented along the principal axes of the elliptic constant-energy surfaces. We will consider weak electric fields $\mathbf{E}$ and weak thermal gradients $\boldsymbol{\nabla} T$ oriented in the plane of the quantum wells. These fields will not in general lie along the principal axes of the assumed elliptic energy surfaces. Thus, the currents will in general not be along the direction of the applied perturbations. The transport coefficients are, however, independent of the magnitudes of $\mathbf{E}$ and $\boldsymbol{\nabla} T$ for small values of these quantities.[12] We first evaluate the coefficients for the directions of the principal axes and then obtain them for arbitrary directions by adding the contributions from the components of the field and temperature gradient in these principal axis directions.

Following Ref. 12, for $\mathbf{E}$ and $\boldsymbol{\nabla} T$ along one of the principal axes, taken to be the x direction, the distribution function for the nth superlattice subband can be expressed in terms of its deviation δf_{nk} from the equilibrium (Fermi) distribution f_0, $f_{n\mathbf{k}}=f_0+\delta f_{n\mathbf{k}}$, with

$$\delta f_{n\mathbf{k}}=\left(\frac{\partial f_0}{\partial\epsilon}\right)\frac{\hbar k_x}{m_x}\left(eE_x\tau_{1n}(\mathbf{k})+\frac{1}{T}\frac{dT}{dx}\tau_{2n}(\mathbf{k})\right). \tag{5}$$

In quantum well systems, the scattering functions $\tau_{1n}(\mathbf{k})$ and $\tau_{2n}(\mathbf{k})$ are anisotropic because of the superlattice band structure $\epsilon_n(k_z)$ along the growth direction, and because of any underlying anisotropy of the bulk band structure. Substituting Eq. (5) into the Boltzmann equation leads to two sets of coupled equations for the scattering functions:

$$L_c(\tau_{1n}(\mathbf{k}))=1,\quad L_c(\tau_{2n}(\mathbf{k}))=\epsilon-\mu, \tag{6}$$

$$L_c(\{\tau_{in}(\mathbf{k})\})=\sum_{n'}\int d\mathbf{k}'W_{nn'}(\mathbf{k},\mathbf{k}')\left(\frac{1-f_{0n'}(\mathbf{k}')}{1-f_{0n}(\mathbf{k})}\right)\times\left(\tau_{in}(\mathbf{k})-\frac{k_x'}{k_x}\tau_{in'}(\mathbf{k}')\right). \tag{7}$$

These coupled equations are analogous to those obtained for isotropic bulk materials.[12,13] They are extended here to include multiple superlattice subbands and anisotropy.

We consider here the scattering of electrons by (1) acoustic phonons via the deformation potential (DP) interaction, and (2) polar optical phonons (POP's) via the Fröhlich interaction. These are the dominant scattering mechanisms at room temperature. We take the phonons to be unaffected by the superlattice structure and the electrons to have modified superlattice wave functions. In quantum wells and wires the scattering rates by optic phonons have been shown to be given to a good approximation by bulk plane waves for the phonons,[14,15] and the superlattice periodicity has only small effects on the acoustic phonons. We take the optic phonon branch to be dispersionless and given by its zone center value $\hbar\omega_0$, and the acoustic branch is taken to be linear with an averaged isotropic velocity $v_0=(3C_{11}+2C_{12}+4C_{44})/5$.[16] The electron-phonon scattering probabilities for quantum well superlattices are

$$W^{\mathrm{POP}}_{nn'}(\mathbf{k},\mathbf{k}')=\frac{2\pi}{\hbar}(N_0+\tfrac{1}{2}\pm\tfrac{1}{2})C^2_{\mathrm{POP}}M^{\mathrm{POP}}_{nn'}(\mathbf{k},\mathbf{k}')\,\delta(\epsilon_{n'}(\mathbf{k}')-\epsilon_n(\mathbf{k})\pm\hbar\omega_0), \tag{8}$$

$$M^{\mathrm{POP}}_{nn'}(\mathbf{k},\mathbf{k}')=\sum_m \frac{|F_{nk_zn'k'_z}(K_m)|^2}{\Delta k_x^2+\Delta k_y^2+(\Delta k_z+K_m)^2},$$

$$C^2_{\mathrm{POP}}=\frac{2\pi e^2}{\kappa^* V}\omega_0. \tag{9}$$

Here, the + (−) sign is for emission (absorption), $\Delta k_i=k'_i-k_i$, $i=x,y,z$, $K_m=2\pi m/d$ is the reciprocal superlattice vector, $1/\kappa^*=1/\kappa_\infty-1/\kappa_0$, $\kappa_0(\kappa_\infty)$ is the static (high-frequency) dielectric constant, and $N_0=1/[\exp(\hbar\omega_0/k_BT)-1]$. The superlattice overlap factor

$$F_{nk_zn'k'_z}(K_m)=\int_0^d e^{i(k'_z-k_z-K_m)z}\Psi^*_{n'k'_z}(z)\Psi_{nk_z}(z)dz \tag{10}$$

is given in terms of the superlattice Bloch functions $\psi_{nk_z}(z)=e^{ik_zz}u_{nk_z}(z)$ with $u_{nk_z}(z+d)=u_{nk_z}(z)$. These functions can be expressed in closed form,[17] which allows the overlap factor to be expressed analytically. At room temperature, the average electron energy is considerably larger than that of acoustic phonons involved in the deformation potential scattering. Thus the scattering probability for this mechanism is, to good approximation, elastic, and has the form

$$W^{\mathrm{DP}}_{nn'}(\mathbf{k},\mathbf{k}')=\frac{2\pi}{\hbar}C^2_{\mathrm{DP}}M^{\mathrm{DP}}_{nn'}(k_z,k'_z)\,\delta(\epsilon_{n'}(\mathbf{k}')-\epsilon_n(\mathbf{k})), \tag{11}$$

$$M^{\mathrm{DP}}_{nn'}(k_z,k'_z)=\sum_m |F_{nk_zn'k'_z}(K_m)|^2,\quad C^2_{\mathrm{DP}}=\frac{E_1^2k_BT}{2V\rho v_0^2}. \tag{12}$$

Introducing the scattering rates Eqs. (8)–(12) into Eqs. (6) and (7) and integrating over the energy conserving δ functions yields the set of coupled ladder equations for $\tau_{1n}(\mathbf{k})$ and $\tau_{2n}(\mathbf{k})$ and

$$\xi_i=S^0_\alpha(\epsilon)\tau_{i\alpha}(\epsilon)-\sum_{\alpha'}S^+_{\alpha\alpha'}(\epsilon)\tau_{i\alpha'}(\epsilon+\hbar\omega_0)-\sum_{\alpha'}S^-_{\alpha\alpha'}(\epsilon)\tau_{i\alpha'}(\epsilon-\hbar\omega_0), \tag{13}$$

where $\alpha=(n,\theta,k_z)$ with $\theta=\tan^{-1}(k_y/k_x)$ and $\xi=1$ for $i=1$ and $\epsilon-\mu$ for $i=2$. These equations are solved using an extension of the Ritz iterative method.[12] This method along with the expressions for the S's in Eq. (13) is presented in the Appendix.

For each valley, the x direction is taken along the semimajor axis of the energy ellipse. The contributions to the electric and heat currents flowing in the superlattice from each valley are given by

$$J_{ex}=-e\sum_n\int\frac{d\mathbf{k}}{4\pi^3}\frac{\hbar k_x}{m_x}\delta f_{n\mathbf{k}}, \tag{14}$$

$$J_{Qx}=\sum_n\int\frac{d\mathbf{k}}{4\pi^3}\frac{\hbar k_x}{m_x}\delta f_{n\mathbf{k}}(\epsilon-\mu) \tag{15}$$

with $\delta f_{n\mathbf{k}}$ given from Eq. (5). These are related to the transport coefficients by

$$J_{ex}=\sigma E_x-\sigma S\frac{dT}{dX}, \tag{16}$$

$$J_{Qx}=\sigma STE_x-\gamma_e\frac{dT}{dX}, \tag{17}$$

where σ and S are the electrical conductivity and Seebeck coefficient and γ_e is the electrical component of the thermal conductivity at zero electric field. It is related to the electrical component of the thermal conductivity at zero current by $\kappa_e=\gamma_e-\sigma S^2T$. The contributions from each valley to the transport coefficients for fields along this direction are

$$\sigma=\frac{e^2k_BT}{m_x}\frac{(m_xm_y)^{1/2}}{\pi\hbar^2d}\sum_n I_{0n}(\mu,T), \tag{18}$$

$$\sigma S=\frac{-ek_B^2T}{m_x}\frac{(m_xm_y)^{1/2}}{\pi\hbar^2d}\sum_n I_{1n}(\mu,T), \tag{19}$$

$$\gamma_e=\frac{k_B^3T^2}{m_x}\frac{(m_xm_y)^{1/2}}{\pi\hbar^2d}\sum_n I_{2n}(\mu,T), \tag{20}$$

where

$$I_{0n}(\mu,T)=\frac{1}{2\pi}\int_{-\pi}^{\pi}d\eta\int_0^\infty d\xi\, f_0\frac{d}{d\xi}[\xi\chi_{1n}(\xi,\eta)], \tag{21}$$

$$I_{1n}(\mu,T)=\frac{1}{2\pi}\int_{-\pi}^{\pi}d\eta\int_{0}^{\infty}d\xi\, f_0\frac{d}{d\xi}\{\xi[\xi-\zeta_n(\eta)]\chi_{1n}(\xi,\eta)\}, \tag{22}$$

$$I_{2n}(\mu,T)=\frac{1}{2\pi}\int_{-\pi}^{\pi}d\eta\int_{0}^{\infty}d\xi\, f_0\frac{d}{d\xi}\{\xi[\xi-\zeta_n(\eta)]\chi_{2n}(\xi,\eta)\}, \tag{23}$$

and

$$\chi_{in}(\xi,\eta)=\frac{1}{\pi}\int_{0}^{2\pi}d\theta\cos^2\theta\,\tau_{in}(\xi,\eta,\theta) \tag{24}$$

with $\eta=k_z d$, $\xi=[\epsilon-\epsilon_n(k_z)]\beta$, $f_0=f_0[\xi,\zeta_n(k_z)]$, and where $\zeta_n(k_z)=[\mu-\epsilon_n(k_z)]\beta$ is the scaled chemical potential. The full transport coefficients are obtained by adding the contributions for all valleys and averaging over the directions of the field and temperature gradient, as is described in Sec. IV for PbTe systems. From these results the power factor $P=\sigma S^2$ is obtained. Equations (18)–(20) reduce to those in the CRTA,[5,6] if we take $\tau_{1n}=\tau$ and $\tau_{2n}=(\epsilon-\mu)\tau$, where τ is a constant relaxation time.

III. THERMOELECTRIC TRANSPORT IN QUANTUM WIRE SUPERLATTICES

For quantum wire superlattices, the Boltzmann equation can again be cast in the form of Eqs. (6) and (7). The wire superlattice dispersion for each valley is

$$\epsilon_n(\mathbf{k})=\epsilon_n(k_y,k_z)+\frac{\hbar^2k_x^2}{2m_x}. \tag{25}$$

Here, $\epsilon_n(k_y,k_z)$ is the quantum wire superlattice dispersion, which is obtained along with the corresponding Bloch functions through solution of the Schrödinger equation for the 2D periodic Kronig-Penny potential with offset V_0. The lack of separability of the Schrödinger equation precludes a closed form solution. Instead, we expand the wire superlattice Bloch functions $\psi_{n\mathbf{k}_\perp}(\boldsymbol{\rho})=e^{i\mathbf{k}_\perp\cdot\boldsymbol{\rho}}u_{n\mathbf{k}_\perp}(\boldsymbol{\rho})$ in a basis of products of quantum well superlattice Bloch states, $u_{n\mathbf{k}_\perp}(\boldsymbol{\rho})=\Sigma_{n_1n_2}C_{n\mathbf{k}_\perp}(n_1,n_2)u_{n_1k_y}(y)u_{n_2k_z}(z)$, where $u_{n_1k_y}(y)$ and $u_{n_2k_z}(z)$ are the Bloch functions for the 1D periodic potential already described in the previous section, and solve the resulting matrix equation for the $c_{n\mathbf{k}_\perp}$.

The electron-phonon scattering probabilities for quantum wire superlattices have a form similar to that for quantum well superlattices but have a 2D reciprocal lattice:

$$M^{\mathrm{POP}}_{nn'}(\mathbf{k},\mathbf{k}')=\sum_{m_1,m_2}\frac{|F_{n\mathbf{k}_\perp n'\mathbf{k}_\perp}(K_{m_1},K_{m_2})|^2}{\Delta k_x^2+(\Delta k_y+K_{m_1})^2+(\Delta k_z+K_{m_2})^2}, \tag{26}$$

$$M^{\mathrm{DP}}_{nn'}(\mathbf{k}_\perp,\mathbf{k}'_\perp)=\sum_{m_1,m_2}|F_{n\mathbf{k}_\perp n'\mathbf{k}_\perp}(K_{m_1},K_{m_2})|^2 \tag{27}$$

with the overlap factor

$$F_{n\mathbf{k}_\perp n'\mathbf{k}'_\perp}(\mathbf{K})=\int_{\mathrm{cell}}e^{i(\mathbf{k}'_\perp-\mathbf{k}_\perp-\mathbf{K})\cdot\boldsymbol{\rho}}\Psi^*_{n'\mathbf{k}'_\perp}(\boldsymbol{\rho})\Psi_{n\mathbf{k}_\perp}(\boldsymbol{\rho})d\boldsymbol{\rho}. \tag{28}$$

The solution of the inelastic multisubband Boltzmann equation for quantum wire superlattices is cast in the form of Eq. (13), with $\alpha=(n,k_y,k_z)$. The solution of this equation is described further in the Appendix.

The contributions for each valley to the transport coefficients for fields along the x direction are

$$\sigma=\frac{2e^2}{\pi m_x d^2}\left(\frac{2m_xk_BT}{\hbar^2}\right)^{1/2}\sum_n I_{0n}(\mu,T), \tag{29}$$

$$\sigma S=-\frac{2ek_B}{\pi m_x d^2}\left(\frac{2m_xk_BT}{\hbar^2}\right)^{1/2}\sum_n I_{1n}(\mu,T), \tag{30}$$

$$\gamma_e=\frac{2ek_B^2T}{\pi m_x d^2}\left(\frac{2m_xk_BT}{\hbar^2}\right)^{1/2}\sum_n I_{2n}(\mu,T), \tag{31}$$

where

$$I_{0n}(\mu,T)=\frac{1}{(2\pi)^2}\int_{-\pi}^{\pi}d\eta\int_{-\pi}^{\pi}d\phi\int_{0}^{\infty}d\xi\, f_0\frac{d}{d\xi}\times[\xi^{1/2}\tau_{1n}(\xi,\eta,\phi)], \tag{32}$$

$$I_{1n}(\mu,T)=\frac{1}{(2\pi)^2}\int_{-\pi}^{\pi}d\eta\int_{-\pi}^{\pi}d\phi\int_{0}^{\infty}d\xi\, f_0\frac{d}{d\xi}\times\{\xi^{1/2}[\xi-\zeta_n(\eta,\phi)]\tau_{1n}(\xi,\eta,\phi)\}, \tag{33}$$

$$I_{2n}(\mu,T)=\frac{1}{(2\pi)^2}\int_{-\pi}^{\pi}d\eta\int_{-\pi}^{\pi}d\phi\int_{0}^{\infty}d\xi\, f_0\frac{d}{d\xi}\times\{\xi^{1/2}[\xi-\zeta_n(\eta,\phi)]\tau_{2n}(\xi,\eta,\phi)\} \tag{34}$$

with $\eta=k_yd$, $\phi=k_zd$, $\xi=[\epsilon-\epsilon_n(k_y,k_z)]\beta$, $f_0=f_0[\xi,\zeta_n(k_y,k_z)]$, and where $\zeta_n(k_y,k_z)=[\mu-\epsilon_n(k_y,k_z)]\beta$ is the scaled chemical potential. The full transport coefficients and the power factor for a field are obtained as described at the end of the previous section.

IV. RESULTS AND DISCUSSION

The present approach is generally applicable to all quantum well superlattice systems. In the following, we illustrate the present treatment of the thermoelectric transport principally with results for PbTe quantum well and quantum wire superlattices, which are of current interest for thermoelectric applications. All results here are for $T=300\,\mathrm{K}$. PbTe is a multivalley system with fourfold degeneracy and with considerable anisotropy in the conduction band in the bulk. The material parameters for PbTe are taken to be $m_l=0.35$, $m_t=0.034$, and $E_1=25\,\mathrm{meV}$, $\hbar\omega_0=14\,\mathrm{meV}$, $\kappa_0=414$, $\kappa_\infty=33$, $C_{11}=1.072\times10^7\,\mathrm{N/cm^2}$, $C_{12}=7.68\times10^5\,\mathrm{N/cm^2}$, and $C_{44}=1.322\times10^6\,\mathrm{N/cm^2}$.[18,19]

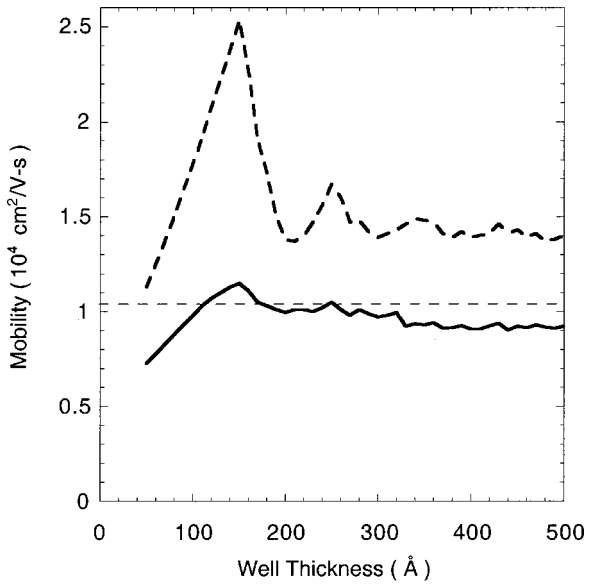

FIG. 1. Carrier mobility due to polar optical phonon scattering for GaAs quantum wells with $V_0=\infty$ as a function of well width in a relaxation time approximation (dashed line) and from the inelastic solution of the Boltzmann equation (solid line). The thin dashed line gives the bulk value. The carrier density is $10^{18}\,\mathrm{cm}^{-3}$.

In order to elucidate the underlying physics it will be helpful to compare these results for PbTe with those from a system with a simpler band structure, GaAs. GaAs has a single isotropic conduction band valley, and the material parameters used for it in the calculations are $m_x=m_y=m_z=0.0665$, $E_1=7$ meV, $\hbar\omega_0=36$ meV, $\kappa_0=12.9$, $\kappa_\infty=10.92$, and $\rho v_0^2=875\,\mathrm{meV/\AA}^3$.

In GaAs POP scattering dominates carrier scattering at room temperature. This is to be contrasted with PbTe in which POP scattering and DP scattering give comparable contributions to the room temperature carrier scattering. To see the physics, it will also be helpful to consider the limit of infinite potential barriers, $V_0=\infty$. In this limit, the superlattice subbands become dispersionless, and the scattering probabilities for wells and wires can be reduced to simpler forms.[20,21]

Figure 1 illustrates the importance of including a full inelastic treatment of the carrier scattering in the Boltzmann equation. It gives calculations of the room temperature POP-limited carrier mobility in GaAs single quantum wells with $V_0=\infty$ as a function of well thickness. The carrier density has been taken to be $10^{18}\,\mathrm{cm}^{-3}$. The dashed line is from a relaxation time approximation in which $\hbar\omega_0$ in the scattering functions from Eq. (13) is neglected.[22] The solid line is from the solution of the full inelastic Boltzmann equation. It is evident from the figure that the relaxation time approximation gives a significantly higher mobility than that obtained from the inelastic calculation for wells with $a\sim 100-200\,\mathrm{\AA}$. This relaxation time approximation neglects the intra- and intersubband inelastic scattering, which reduce the mobility. This in turn will give lower thermoelectric power factors.

The decrease in mobility in both curves in Fig. 1 for decreasing a below 150Å arises from the increase in the scattering rates with decreasing widths. For large well widths, the contributions from many subbands converge, and the bulk value (thin dashed line) is recovered. The lower mobilities obtained from the inelastic treatment for large well widths are in agreement with the measured bulk mobilities in GaAs,[23] and point to the importance of an inelastic treatment to accurately describe carrier transport in lower-dimensional systems.

PbTe is a good room temperature thermoelectric material in bulk with a $ZT\sim 0.4$. Its thermoelectric properties have also been studied in PbTe/PbEuTe quantum well systems,[8,9] and enhanced power factors were observed in them. Bulk PbTe has four highly anisotropic ellipsoidal valleys along the [111] crystallographic directions. Here, we consider PbTe quantum well superlattices with growth axes along [111] and [100] directions. For the [111] direction, the confinement lifts the fourfold valley degeneracy resolving one set of minibands from the longitudinal valley lying below another threefold degenerate set of subbands from the oblique valleys. In the [001] orientation, the masses for all four valleys along the confinement direction are the same. Superlattices in this orientation retain the fourfold valley degeneracy of the bulk.

For the [111] orientation, the in-plane subband structure for the longitudinal valley is isotropic and the contribution to transport from this valley is obtained by setting in the above equations $m_x=m_y=m_t=0.034$, $m_z=m_l=0.35$. For each of the three oblique valleys, the contribution to the conductivity has the form $\frac{1}{2}(\sigma_x+\sigma_y)$, where σ_x is given by Eq. (18) with $m_x=0.034$, $m_y=0.172$, $m_z=0.038$, while σ_y is obtained with $m_x=0.172$, $m_y=0.034$, $m_z=0.038$.[24] For the [001] orientation, the confinement mass is $m_z=0.049$ for all four valleys, and the contribution to the conductivity for each valley is again $\frac{1}{2}(\sigma_x+\sigma_y)$ with $m_x=0.085$ and $m_y=0.034$ for σ_x and $m_x=0.034$ and $m_y=0.085$ for σ_y. Analogous evaluations are made for σS and γ_e from Eqs. (19) and (20). From these results the total transport coefficients and the power factor $P=\sigma S^2$ are obtained by summing over all valleys.

P is always a function of carrier density, and in all of the following we evaluate P at the densities for which P is a maximum. In Fig. 2, P is shown for [100] PbTe quantum well superlattices with $V_0=\infty$ and $b=0$ using several treatments of the carrier scattering. P is scaled to the bulk value for the same treatment of carrier scattering. Previous calculations within the CRTA for similar systems with strong confinement[3,4] have suggested that P should increase monotonically with decreasing well and wire widths, attaining values well above the bulk value. This behavior is given by the dash-dotted line in Fig. 2. The dotted line gives P with carrier scattering by only optic phonons. The dashed curve shows P with only scattering of carriers by acoustic phonons, which is independent of well width. To see why P is independent of a in this case, we note that in the high-temperature approximation to DP scattering,[12] which is valid for PbTe at room temperature, the carrier relaxation time for this fully confined case, τ, is inversely proportional to the density of electronic states per unit volume, D, which itself varies as $1/a$. Since $\sigma\sim D\tau$, it becomes independent of a for acoustic phonon scattering, and thus P is independent of a.

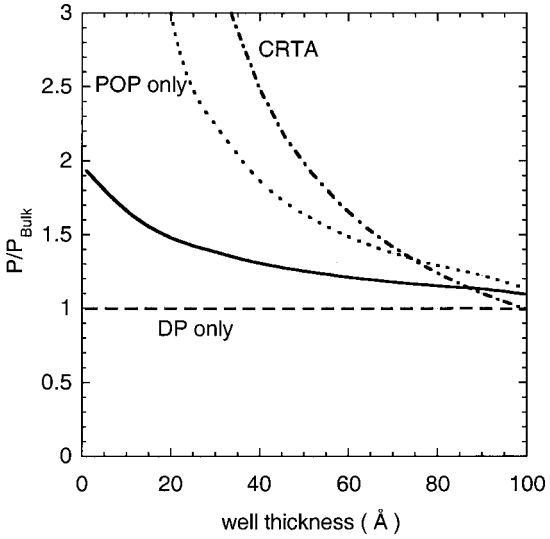

FIG. 2. Power factor P for PbTe [100] quantum well superlattices with $V_0=\infty$ and the barrier width $b=0$ scaled to corresponding bulk value. Different treatments of the carrier scattering are used, as described in text.

The solid line in Fig. 2 shows P including both POP and DP scattering. The relatively weak increase of P with decreasing well thickness reflects the fact that DP scattering increases with decreasing well thickness and becomes dominant in PbTe in strongly confined well geometries as $a\rightarrow 0$, as noted above. These results from the present inelastic treatment are also dramatically different from those in the CRTA and will be seen to have implications for PbTe superlattices with finite V_0, particularly for the dependence on V_0.

Figure 3 shows these same results for P including both POP and DP scattering for PbTe [100] quantum wells with $V_0=\infty$, and corresponding results for GaAs. Here, the semilogarithmic plot extends over a wider range of well widths. For both cases, at large well widths, P approaches the bulk

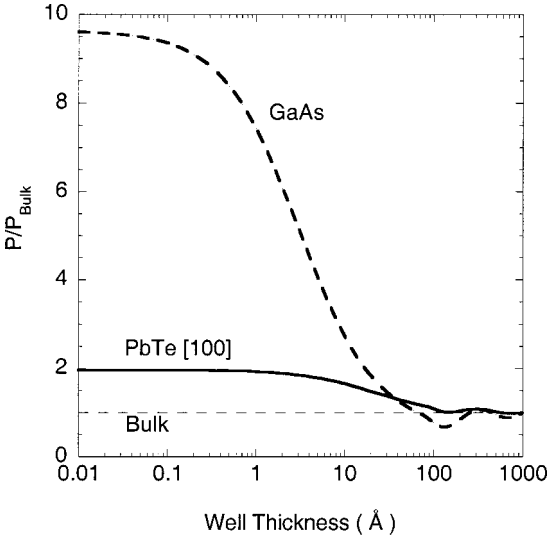

FIG. 3. Power factors P for PbTe [100] and GaAs quantum well superlattices with $V_0=\infty$ and $b=0$ scaled to corresponding bulk P's as a function of well width.

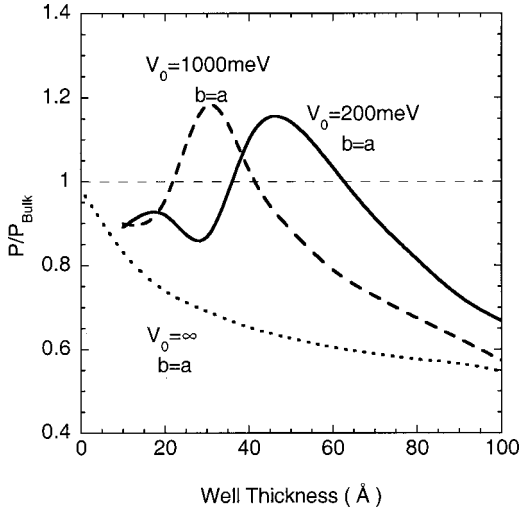

FIG. 4. Power factor for PbTe [100] quantum well superlattices with $b=a$ as a function of well thickness for several values of V_0.

value. To obtain this limit correctly, many 2D subbands had to be included, and the convergence of our results for quantum wells as $a\rightarrow\infty$ to the bulk result demonstrates the accuracy of the numerical treatment used here. For narrow wells, P for each material approaches a constant value, reflecting the dominance of the DP scattering as $a\rightarrow 0$ for infinite potentials, as discussed above. The weak DP scattering in GaAs causes this limiting value of P to be much larger than for PbTe.

We now consider superlattices with finite potential barriers. Figure 4 gives the results for [100] PbTe quantum wells with $b=a$ and increasing V_0. The dependence on a here is similar to that already found in calculations using the CRTA.[5,6] For wide wells P lies below the bulk value. This arises because the charge carriers are constrained to flow preferentially through the quantum wells, resulting in a decreased current per total unit area as compared to bulk and in a decreased P. For decreasing a,P increases, reaches a maximum, and then decreases again due to tunneling. This behavior is a consequence of the increased effects of carrier tunneling through barriers as $a\rightarrow 0$. The enhancement of P over the bulk value arises from the changes in the carrier density of states upon electron confinement in relatively narrow wells.

An important difference between the present results and the earlier results from the CRTA is that here the maximum P as a function of a is not much affected by V_0. This point is shown in Fig. 5, where the maxima in the curves of P vs a are given as functions of V_0. In the CRTA, these maxima of P increase with V_0, whereas in the full calculations they are nearly independent of V_0. Physically we find that for increasing V_0 the increased scattering rates due to stronger carrier confinement offset the density of states enhancement, resulting in a weak dependence of P on V_0. To see this increased scattering in more detail, Fig. 6 gives the calculated in-plane mobility as a function of well thickness for a carrier density of $10^{18}\,\mathrm{cm}^{-3}$. For $V_0=200\,\mathrm{meV}$, the effects of confinement are small, and the mobility remains near the bulk value. With increasing V_0 the mobility decreases due to

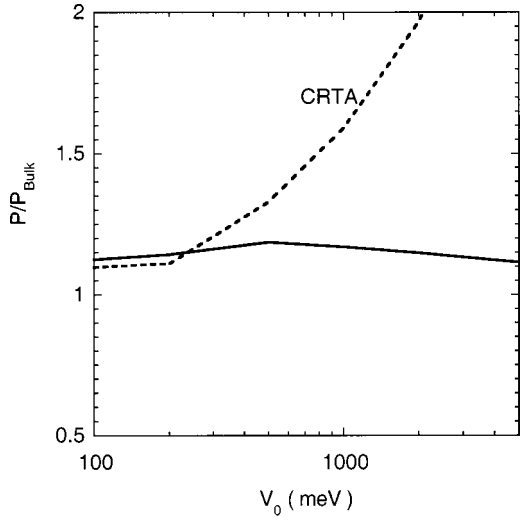

FIG. 5. Maxima taken from P vs a curves for [100] PbTe quantum well superlattices as a function of potential offset V_0 for equal well and barrier widths ($b=a$). Solid curve is from inelastic treatment and dotted line is from the constant relaxation time approximation.

the increased scattering rates produced by confinement. Thus, for $V_0=1000\,\mathrm{meV}$, the mobility is closer to that for $V_0=\infty$ for large well widths, but it approaches the bulk value for narrow wells where carrier tunneling becomes important.

GaAs provides an example of a bulk material in which the room temperature scattering rates from POP's are larger compared to those of DP scattering by acoustic phonons. Figure 7 shows the maxima in the curves of P as a function of a plotted vs V_0 for GaAs quantum well superlattices. The solid line gives the results from the full calculation, and the dashed line gives the results for the CRTA. As was true for PbTe (see Fig. 5), here P is quite insensitive to V_0. Although

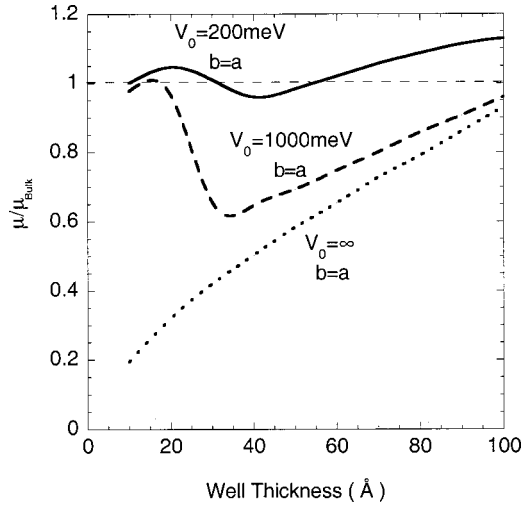

FIG. 6. Carrier mobility for PbTe [100] quantum wells scaled to the bulk value as a function of well thickness for several values of V_0.

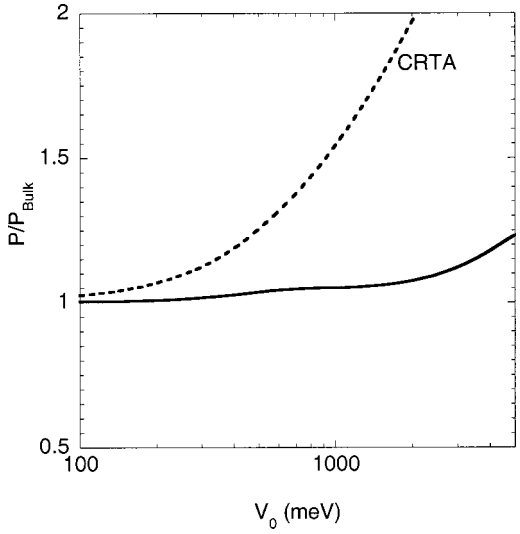

FIG. 7. Maxima taken from P vs a curves for GaAs quantum well superlattices as a function of potential offset V_0 for equal well and barrier widths ($b=a$). Solid curve is from inelastic treatment and dotted line is from the constant relaxation time approximation.

the POP interaction leads to an increase in P for $V_0\rightarrow\infty$ and $a\rightarrow 0$ as seen in Fig. 3, this does not occur in the more realistic region of parameter space considered in Fig. 7. Thus for PbTe and GaAs quantum well superlattices we conclude that the dependence of P on V_0 is relatively weak. We suggest that this behavior will be found to be typical of semiconductor superlattices.

PbTe [111] quantum well superlattices provide an example of systems in which the degeneracy of the conduction bands is lifted with increasing potential offset, leading to interesting changes in the power factor. Figure 8 shows P as a function of a for [111] PbTe quantum well superlattices with $b=a$ and with three different barrier heights. For weaker confinement, $V_0=200\,\mathrm{meV}$, the valley degeneracy is not much lifted, causing P to lie closer to the bulk value. With increasing V_0 the conduction band valley degeneracy is

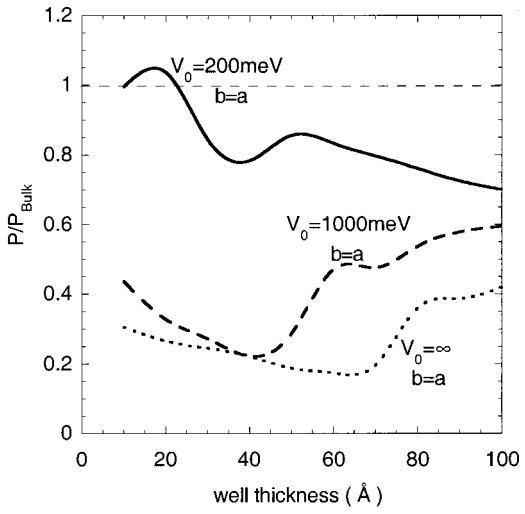

FIG. 8. P as a function of a for [111] PbTe quantum well superlattices with $b=a$ and three different barrier heights.

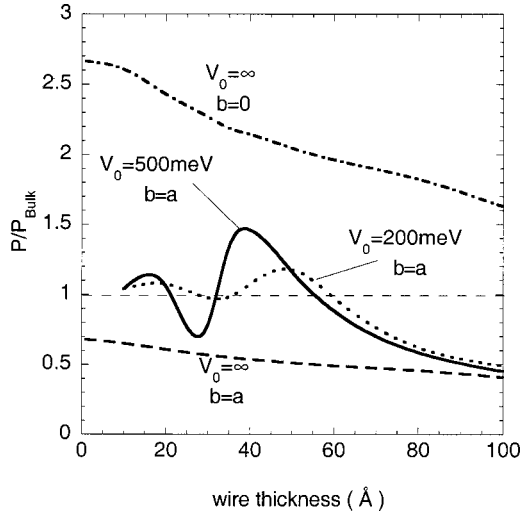

FIG. 9. Power factors P vs wire width a for [100] quantum wire superlattices described in text with potential offsets and barrier widths indicated.

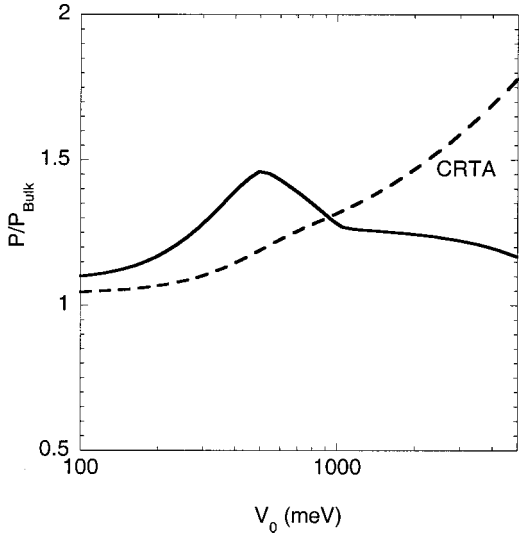

FIG. 10. Maxima from P vs a curves for [001] PbTe quantum wire superlattices as functions of potential offset V_0 for equal well and barrier widths ($b=a$). Solid curve is from the inelastic treatment and dashed line is from the constant relaxation time approximation.

increasingly lifted. This results in fewer valleys contributing to conduction and in a corresponding reduction of P.

We now turn to quantum wire superlattices and consider PbTe wire systems with two orientations. We find that quantum wire superlattices have qualitatively different behaviors in some respects than do quantum well superlattices. For the ''[100]'' quantum wire superlattices, the confinement directions are taken to be [001] and [010], and the transport direction is taken along [100]. For ''[111]'' quantum wire superlattices, the confinement directions are [111] and $[11\bar{2}]$, and the transport direction is $[1\bar{1}0]$. The valley degeneracy is lifted by confinement in the [111] superlattices, and it is not lifted in the [100] superlattices. The quantum wires are taken to have square cross section and are arranged on a square lattice.

Figure 9 gives P for PbTe [100] quantum wire superlattices. The dependence of P on a is qualitatively similar to that found for this system in the CRTA, as was the case above for the corresponding quantum well superlattices. Once again, for finite V_0, P is smaller than the bulk value for large wire widths, it reaches a maximum for decreasing a, and then it decreases due to carrier tunneling. The dependence on V_0 of the maxima in P as a function of a for PbTe quantum wire superlattices is shown in Fig. 10. In contrast to the quantum well case shown in Fig. 5, these P exhibit a noticeable maximum at $V_0=500$ meV that lies above the CRTA value for the corresponding V_0 and is about 50% over the bulk value. This difference is traced to the form of the inelastic scattering in the one-dimensional geometry. For large values of V_0, the increased scattering rates cause P to drop. Figure 11 gives the corresponding results for GaAs quantum wire superlattices. For this case, a weaker dependence of P on V_0 is observed as compared to the corresponding case of PbTe because of the relatively stronger POP scattering.

Figure 12 shows the power factor for [111] quantum wire superlattices as a function of wire size for different potential offsets. For modest potential offset, $V_0=200$ meV, P remains close to the bulk value because of strong barrier penetration of the carrier wave function. With increasing confinement P decreases due to the lifting of the valley degeneracy, as in the case of PbTe [111] quantum well superlattices discussed above. However, this decrease is not as rapid with increasing barrier height as it is in quantum well superlattices (Fig. 8) for two reasons. First, the strong asymmetry in the bulk band structure combined with the two confinement directions for wires causes the lifting of the valley degeneracy with increasing confinement to be weaker than it is for wells. Sec-

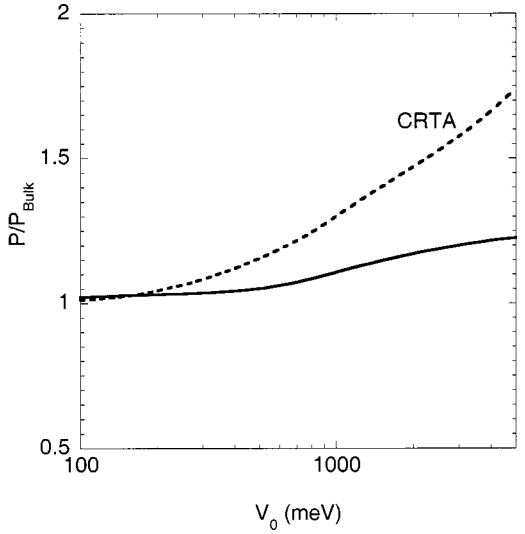

FIG. 11. Maxima taken from P vs a curves for GaAs quantum wire superlattices as functions of potential offset V_0 for equal well and barrier widths ($b=a$). Solid curve is from the inelastic treatment and dashed line is from the constant relaxation time approximation.

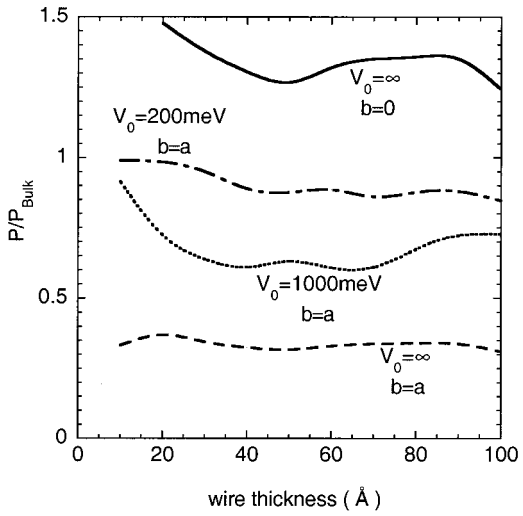

FIG. 12. Power factors P for PbTe [111] quantum wire superlattices described in the text for potential offsets indicated, and well widths equal to barrier widths, $b=a$.

ondly, for a given barrier height the wire wave function spreads more into the barrier region than is true for wells so the approach to the limiting case of $V_0=\infty$, $b=a$ is a weaker function of V_0.

For quantum wire superlattices with $V_0=\infty$, $b=a$, P remains below the bulk value for all a for the case of PbTe (see Fig. 9). For GaAs, P increases modestly and approaches $P/P_{\text{bulk}}\sim 2$ for $a\rightarrow 0$. We note that for the quantum wire superlattices considered here the wire region is only $\frac{1}{4}$ of the full volume of the system, and for $V_0=\infty$ this barrier material strongly reduces P. For corresponding well superlattices the well region is $\frac{1}{2}$ of the system volume. Thus, the barrier material has a more profound effect on thermoelectric transport in wires than in wells.

For quantum wire superlattices with $V_0=\infty$ and $b=0$ the CRTA predicts a divergence in $P(P\sim 1/a^2)$ for $V_0\rightarrow\infty$ and $a\rightarrow 0$.[4] The results presented here show that P remains finite for all a because of the enhancement of carrier scattering in this limit. Still, P for both PbTe and GaAs wire superlattices with $V_0=\infty$ and $b=0$ is much higher than that for superlattices with barrier material present, which suggests that ''free-standing'' quantum wire systems may give high P and high figures of merit ZT. Such quantum wire systems are currently being investigated experimentally.

In summary, we have given a quantitative theoretical description of the power factor for thermoelectric transport in superlattices and have made calculations for PbTe and GaAs quantum well and quantum wire superlattices. These calculations include (i) 3D superlattice band structure used in (ii) a multisubband inelastic Boltzmann equation for carrier transport. We have shown that these two features are needed for a quantitative treatment of thermoelectric transport in superlattice systems. We find that a strong dependence of P on orientation occurs for both PbTe quantum well and quantum wire superlattice systems. It results from the anisotropic multivalley bulk band structure, which causes the effective masses for each valley to depend on the choice of confinement direction and lifts the valley degeneracy along all but special directions. For PbTe quantum well superlattices, we find that the increased carrier scattering rates that occur with increasing confinement cause the power factor to remain near the bulk value for all barrier heights, a result that contrasts strongly with the large enhancements in P predicted from calculations employing the constant relaxation time approximation. For both PbTe and GaAs quantum wire superlattices, only modest increases in P are seen for a wide range of realistic potential offsets. These results lead us to suggest that the features presented here are to be expected for all semiconductor superlattice systems. We suggest here that significant enhancements in P can be achieved only by eliminating the parasitic effect of heat transport through the barrier material, which might be achieved, for example, in free-standing wire systems.

ACKNOWLEDGMENT

This work was supported in part by the U.S. Office of Naval Research.

APPENDIX

Here we first outline the Ritz procedure for systems with isotropic band structure and a single subband.[12,13] In this case, the Boltzmann equation can be reduced to a simpler form than Eq. (13):

$$\xi_i = S^0(\epsilon)\tau_i(\epsilon) - S^+(\epsilon)\tau_i(\epsilon+\hbar\omega_0) - S^-(\epsilon)\tau_i(\epsilon-\hbar\omega_0). \tag{A1}$$

Here, S^0 is the sum of both the out-scattering and in-scattering contributions of all the elastic processes and the out-scattering contributions of the inelastic terms, while S^+ and S^- represent the in-scattering processes due to absorption and emission, respectively. To begin the procedure, the energy variable is discretized with steps whose size is much smaller than the LO phonon energy. The value of τ_i at energy ϵ is connected to a ladder of τ_i's at $\epsilon\pm l\hbar\omega_0$, where l is an integer. On the zeroth iteration, S^+ and S^- are set to zero, giving $\tau_i^{(0)}(\epsilon)=\xi_i/S^0(\epsilon)$. Subsequent iterative values are obtained in terms of previous values as

$$\tau_{i\alpha}^{(m)}(\epsilon) = \frac{\xi_i + \Sigma_{\alpha'} S^+_{\alpha\alpha'}(\epsilon)\tau_{i\alpha'}^{(m-1)}(\epsilon-\hbar\omega_0) + \Sigma_{\alpha'} S^-_{\alpha\alpha'}(\epsilon)\tau_{i\alpha'}^{(m-1)}(\epsilon-\hbar\omega_0)}{S^0_\alpha(\epsilon)}. \tag{A2}$$

The S's and τ's in Eq. (A2) are valid for arguments $\geqslant \epsilon_{n'}(\mathbf{k}')$. The expressions for the S's are

$$S^0_\alpha(\epsilon)=\sum_{\alpha'}\left[S^{0+}_{\alpha\alpha'}(\epsilon)+S^{0-}_{\alpha\alpha'}(\epsilon)\right]+S^{0,ac}_{nk_z}(\epsilon) \tag{A3}$$

with

$$S^{0\pm}_{\alpha\alpha'}(\epsilon)=(N_0+\tfrac{1}{2}\pm\tfrac{1}{2})\,\gamma_{\rm POP}\frac{1-f_0(\epsilon\pm\hbar\omega_0)}{1-f_0(\epsilon)}M^{\rm POP}_{nn'}(\mathbf{k},\mathbf{k}') \times\Theta(\epsilon\pm\hbar\omega_0-\epsilon_{n'}(k_z'))\Delta k_z\Delta\theta, \tag{A4}$$

and

$$S^{0,ac}_{nk_z}(\epsilon)=\gamma_{ac}\sum_{n',k_z'}M^{\rm DP}_{nn'}(k_z,k_z')\Theta(\epsilon-\epsilon_{n'}(k_z'))\Delta k_z\,. \tag{A5}$$

Here, $M^{\rm POP}_{nn'}(\mathbf{k},\mathbf{k}')$ and $M^{\rm DP}_{nn'}(k_z,k_z')$ are taken from Eqs. (9) and (12), respectively, with

$$\gamma_{\rm POP}=\frac{e^2}{2\pi\kappa^*}\frac{(m_xm_y)^{1/2}}{\hbar^2}\omega_0,\quad \gamma_{ac}=\frac{E_I^2}{2\pi\rho v_l^2}\frac{(m_xm_y)^{1/2}}{\hbar^2}\frac{k_BT}{\hbar}. \tag{A6}$$

In Eq. (A4), $\mathbf{k}'=(k_{x\pm},k_{y\pm},k_z')$ with $k_{x\pm}$ and $k_{y\pm}$ given by

$$k_{x\pm}=\left(\frac{2m_x}{\hbar^2}\right)^{1/2}[\epsilon\pm\hbar\omega_0-\epsilon_{n'}(k_z')]^{1/2}\cos\theta',$$

$$k_{y\pm}=\left(\frac{2m_y}{\hbar^2}\right)^{1/2}[\epsilon\pm\hbar\omega_0-\epsilon_{n'}(k_z')]^{1/2}\sin\theta', \tag{A7}$$

and Θ is the Heaviside step function; Δk_z and $\Delta\theta$ are the weighting factors for the quadrature over k_z and θ. The in-scattering processes due to POP absorption and emission are related to Eq. (A4) as

$$S^{\pm}_{\alpha\alpha'}(\epsilon)=S^{0\pm}_{\alpha\alpha'}(\epsilon)\frac{k_{x\pm}}{k_x}. \tag{A8}$$

For quantum wire superlattices, a similar iterative procedure is used. Now, the quadrature is over the 2D superlattice variables k_y' and k_z', which range from $-\pi/d$ to π/d. The expressions for the S's become

$$S^{0\pm}_{\alpha\alpha'}(\epsilon)=(N_0+\tfrac{1}{2}\pm\tfrac{1}{2})\,\gamma_{\rm POP}\frac{1-f_0(\epsilon\pm\hbar\omega_0)}{1-f_0(\epsilon)}[M^{\rm POP}_{nn'}(\mathbf{k},\mathbf{k}'_+) +M^{\rm POP}_{nn'}(\mathbf{k},\mathbf{k}'_+)]\Theta(\epsilon\pm\hbar\omega_0-\epsilon_{n'}(k_y',k_z'))\Delta k_y\Delta k_z\,, \tag{A9}$$

$$S^{0,ac}_{nk_z}(\epsilon)=\gamma_{ac}\sum_{n',k_y',k_z'}M^{\rm DP}_{nn'}(\mathbf{k},\mathbf{k}')\Theta(\epsilon-\epsilon_{n'}(k_y',k_z')) \times\Delta k_y,\Delta k_z\,, \tag{A10}$$

$$\gamma_{\rm POP}=\frac{e^2}{2\pi\kappa^*}\frac{m_x}{\hbar^2}\omega_0,\quad \gamma_{ac}=\frac{E_1^2}{2\pi^2\rho v_l^2}\frac{m_x}{\hbar^2}\frac{k_BT}{\hbar}. \tag{A11}$$

Here, $M^{\rm POP}_{nn'}(\mathbf{k},\mathbf{k}')$ and $M^{\rm DP}_{nn'}(k_z,k_z')$ are taken from Eqs. (26) and (27) respectively, and $k'_\pm=(\pm k_x',k_y',k_z')$, with $k_x'=k_{x\pm}$ and $k_{x\pm}=(2m_x/\hbar^2)^{1/2}\,[\epsilon\pm\hbar\omega_0-\epsilon_{n'}(k_y',k_z')]^{1/2}$.

[1] G. Mahan, B. Sales, and J. Sharp, Phys. Today **50** (3), 42 (1997).
[2] H. J. Goldsmidt, *Thermoelectric Refrigeration* (Plenum, New York, 1964).
[3] L. D. Hicks and M. S. Dresselhaus, Phys. Rev. B **47**, 12 727 (1993).
[4] L. D. Hicks and M. S. Dresselhaus, Phys. Rev. B **47**, 16 631 (1993).
[5] J. O. Sofo and G. D. Mahan, Appl. Phys. Lett. **65**, 2690 (1994).
[6] D. A. Broido and T. L. Reinecke, Phys. Rev. B **51**, 13 797 (1995).
[7] D. A. Broido and T. L. Reinecke, Appl. Phys. Lett. **67**, 100 (1995).
[8] T. C. Harman, D. L. Spears, and M. J. Manfra, J. Electron. Mater. **25**, 1121 (1996).
[9] L. D. Hicks, T. C. Harman, X. Sun, and M. S. Dresselhaus, Phys. Rev. B **53**, 10 493 (1996).
[10] D. A. Broido and T. L. Reinecke, Appl. Phys. Lett. **70**, 2834 (1997).
[11] T. Koga, T. C. Harman, S. B. Cronin, and M. S. Dresselhaus, Phys. Rev. B **60**, 14 286 (1999).
[12] See, for example, B. R. Nag, *Electron Transport in Compound Semiconductors* (Springer-Verlag, Berlin, 1980).
[13] J. O. Sofo and G. D. Mahan, Phys. Rev. B **49**, 4565 (1994).
[14] H. Rücker, E. Molinari, and P. Lugli, Phys. Rev. B **45**, 6747 (1992).
[15] P. A. Knipp and T. L. Reinecke, Phys. Rev. B **48**, 18 037 (1993).
[16] J. D. Zook, Phys. Rev. A **136**, A869 (1964).
[17] C. Kittel, *Introduction to Solid State Physics*, 6th ed. (Wiley, New York, 1986), Chap. 7.
[18] *Numerical Data and Functional Relationships in Science and Technology*, edited by O. Madelung, New Series, Group III, Landolt-Börnstein, Vol. 17, Pt. e (Springer-Verlag, Berlin, 1982), pp. 218–258.
[19] G. Nimtz and B. Schlicht, *Narrow-Gap Semiconductors* (Springer-Verlag, Berlin, 1982), pp. 1–106.
[20] P. J. Price, Ann. Phys. (N.Y.) **133**, 217 (1981).
[21] J. P. LeBurton, J. Appl. Phys. **56**, 2850 (1984).
[22] T. Tsuchiya and T. Ando, Phys. Rev. B **48**, 4599 (1993).
[23] *Numerical Data and Functional Relationships in Science and Technology*, edited by O. Madelung, New Series, Group III, Landolt-Börnstein, Vol. 17, pt. f. (Springer-Verlag, Berlin, 1982), pp. 170–180.
[24] To obtain these masses, we have chosen the coordinate system with $\hat{x}$ along the $[1\bar{1}0]$ direction, $\hat{y}$ along $[11\bar{2}]$, and $\hat{z}$ along $[111]$.